Integrated Modeling for the Manufacture of Ni-Based Superalloy Discs from Solidification to Final Heat Treatment

S. TIN, P.D. LEE, A. KERMANPUR, M. RIST, and M. McLEAN

Process models of the various stages of gas-turbine disc manufacture have been integrated to simulate the physical and microstructural transformations occurring within a nickel-based superalloy throughout the entire manufacturing route. Production of these critical rotating structural components requires several distinct processing stages: vacuum-induction melting (VIM), vacuum-arc remelting (VAR), homogenization heat treatment, cogging, forging, final heat treatment, and machining. During the course of these consecutive manufacturing stages, the various thermal and thermomechanical processes lead to significant changes in both the microstructural characteristics and internal stresses in the alloy. Although separate models have previously been developed to simulate the individual processing stages, this article describes how these models, which are explicitly expressed in terms of the initial and evolving microstructure, can be integrated to simulate the entire manufacturing process from secondary melting through to the final forging and heat treatment. The grain structure predicted for one stage is explicitly transferred as the initial conditions for the model, which simulates the grain evolution during the next step. This information also provides the basis of microstructure-explicit constitutive equations describing the material behavior. Industrial-scale manufacturing trials associated with the production of an INCONEL alloy 718 aeroengine turbine disc were used to validate the integrated model for grain size. The model also allows intrinsic or extrinsic defects entrained within the material during the initial solidification stage to be tracked through the subsequent processes. This provides a basis for calculating the areas of discs likely to be vulnerable to such defects and whether they might be removed during machining. It was shown that the microstructure of the alloy changes significantly throughout the process chain, the final microstructure and defect distribution at each stage being related to those formed in the previous stages. There was good agreement between the model predictions and experimental observations for both the intermediate and final processing stages. The implications of such integrated modeling for quality assurance through process control are discussed.

I. INTRODUCTION

INCREASINGLY stringent targets for fuel efficiency, engine performance, and emission control in modern gas turbines require structural components to operate under extreme conditions of temperature, atmosphere, and stress. This has led to the use of robust Ni-based superalloy discs as the critical rotating components. These discs need to have exceptional integrity, especially for aerospace applications, where safety is paramount. The quality of a gas-turbine disc is assessed in terms of critical features, such as its grain structure, defect content, mechanical properties, residual stress state, dimensional tolerance, and surface condition.[1] Each processing stage can influence these features and requires tight process control to ensure conformity to the engineering design requirements, significantly impacting the cost of a disc.

This article demonstrates the ability of an integrated, through-process model to simulate the characteristic changes in grain size/morphology associated with the commercial production of Ni-based superalloy discs. With the high-temperature properties of cast/wrought superalloys being highly sensitive to the resultant microstructures,[2] the ability to precisely engineer the grain structure enables further optimization of the structural component. For example, coarse-grained microstructures can be utilized to minimize creep deformation at the gas-turbine disc rim, while refinement of the grains at the bore of the finished disc increases the resistance to fatigue-crack growth/initiation and also provides a significant degree of Hall–Petch strengthening. In addition to the influence on the in-service mechanical performance, control of grain size also affects the thermal-mechanical response during hot working, which can reduce operational costs and improve component integrity.

Typical manufacturing routes for gas-turbine discs consist of seven successive stages.[3] First, vacuum induction melting (VIM) is used to produce an alloyed electrode ingot with tightly controlled composition and low impurity levels. With the resulting properties of these structural materials being highly sensitive to trace elements (such as O, N, S, and C) melting in vacuum assists in minimizing contamination of cast ingots, which often weigh in excess of 5000 kg. To minimize melt-related defects and yield a sound ingot with a microstructure that is amenable to subsequent thermomechanical processing, the ingot produced by VIM is remelted. Vacuum arc remelting (VAR) is the most common secondary remelting process for the production of fully dense

S. TIN, Assistant Director of Research, is with the Rolls-Royce University Technology Partnership, University of Cambridge, Cambridge CB2 3QZ, United Kingdom. Contact e-mail: st298@hermes.ca.ac.uk P.D. LEE, Reader, A. KERMANPUR, Associate Professor, and M. McLEAN, Professor, are with the Department of Materials, Imperial College London, London SW7 2BP, United Kingdom. M. RIST, Lecturer, is with the Department of Materials Engineering, Open University, Milton Keynes MK7 6AA, United Kingdom.

Manuscript submitted November 18, 2004.

and homogeneous ingots of reactive and macrosegregation-sensitive alloys.

Thermomechanical processing of Ni-based superalloy aeroengine discs begins with a homogenization heat treatment of the as-solidified VAR ingot. The heat treatment dissolves the nonequilibrium eutectic phases, reduces the degree of dendritic microsegregation, and modifies the grain structure. Due to the extended high-temperature exposure required for homogenization, significant grain growth occurs during this process.[4] Since the grain size plays a vital role in determining the yield strength and fatigue resistance of high-temperature structural materials, control of these features during processing is critical to the resulting performance of rotating aeroengine components. The process of hot working that converts large cast and homogenized ingots into semi-finished billet products is often referred to as *cogging*. The process typically involves multiple hot-deformation passes through a set of open dies, with rotation and/or reheating of the ingot occurring between passes. As the length of the ingot gradually increases and the diameter decreases during cogging, refinement of the grain structure occurs as the result of various recrystallization mechanisms. The process also enhances the structural integrity of the finished component, as internal microcracks and porosity present in the original ingot are minimized during cogging. Following rigorous inspection of the billet for deleterious inclusions and associated defects, sections of the billet can then be prepared for forging into near-net-shape disc components. In contrast to the cogging process, which involves hundreds of discrete and incremental deformation steps, net-shape forging generally consists of a single hot-deformation step utilizing a set of closed dies. Deformation of the billet material causes the metal to flow and fill the cavity of the shaped dies. Although the principal aim of the forging process is to shape the cogged billet, microstructural control is also required to achieve the integrity and service requirements of the finished component.

After forging, discs are typically subjected to a complex heat treatment followed by machining to the final shape. The postforging heat treatments are designed to optimize the mechanical properties of the forged component. Often performed in two stages, the primary heat treatment modifies the grain structure and assists in refining precipitate sizes and morphologies. Rapid oil or water quenches are often employed to induce uniform precipitation of intermetallic strengthening precipitates throughout the microstructure. Secondary aging treatments are performed at lower temperatures to stabilize the final microstructure and relieve any residual stresses formed on quenching from elevated temperatures. Despite forging the billet to near-net shapes, the intricate structural features present on complex forgings often require substantial amounts of material to be removed (up to 70 pct of the metal) to finish the component. Extremely tight dimensional tolerances are required during machining of these critical rotating components.

Stringent quality-control standards combined with a limited understanding of mechanisms pertaining to defect formation during these processing steps can cause nonconformance that results in a high rejection rate throughout the supply chain. The ability to accurately model the production of aeroengine discs and predict conditions leading to the occurrence of these defects is both academically challenging and industrially relevant. Although each of the separate stages has been modeled previously (*e.g.* VAR,[5–11] homogenization,[12,13,14] cogging,[15] and forging,[16,17]), little effort has been directed toward *integrated modeling* of the full processing route. An integrated process model could be a powerful tool for optimizing production routes and engineering desirable properties. The interest in this type of tool is illustrated by the existence of a number of collaborative research projects striving for the same goal for other processing routes (*e.g.*, CTMP,[18] VIR-CAST/FORM/FAB,[19] and that of Maijer *et al.*[20]).

This investigation is part of a six-partner collaboration, referred to as Integrated Modeling for the Manufacture of Aerospace Discs, that involved both universities and manufacturing companies. Its aim was to develop an integrated process model to simulate both microstructural changes and defect tracking during the manufacture of gas-turbine discs. The modeling procedures for each of the individual process stages are first described. Comparisons between numerical simulations and experimental observations are made where possible. The approach for transferring microstructural information between the various stages is also discussed. Finally, the capabilities of the integrated process model are demonstrated by tracking potential melt-related defects through the entire manufacturing route and predicting their final location in the finished forging.

II. MODEL THEORY FOR THE INDIVIDUAL PROCESSES

A. *Vacuum-Induction Melting*

Since the alloyed ingot produced by VIM is remelted during the subsequent VAR process, generic microstructural information, such as the cast grain structure, will not influence subsequent processing. However, extrinsic defects, such as particles or fragments of the vacuum-induction-melted electrode, may fall into the VAR melt pool and become entrapped within the mushy zone. Particles which survive this process are often referred to as *white spots* in the final ingot.[21,22,23] Knowledge of the particle distributions and other heterogeneous features of ingots produced by VIM (*e.g.*, coarse dendrites in the shrinkage pipe) are necessary to simulate the formation of such white spots.[9,24]

B. *Vacuum-Arc Remelting*

A multiscale model has been developed to simulate the VAR process. The model combines a macroscopic solution of the heat transfer, fluid flow, solidification, and electromagnetic forces using the Specialty Metals Processing Consortium's (Sandia National Laboratories, Albuquerque, NM) VAR finite-difference package[25,26] coupled to a mesoscale cellular automaton (CA) model of grain nucleation and growth.[27–30] Details of the multiscale model have been described elsewhere.[3,11] In the macromodel, input power, defined as the power supply current multiplied by the machine voltage measured at the buss bars ($P_{\text{total}} = I_b V_b$) is automatically balanced against several sources of energy dissipation. This total power is considered to be the sum of the power required to raise the metal to its superheat temperature, the thermal energy lost directly to the crucible wall, and

the thermal energy transmitted to the top surface of the pool by the arc. The first term is related to the steady-state melt rate of the process. The second term depends on the fraction of the input current that passes directly from the crucible or crown to the electrode generating anodic surface heating at the crucible wall. The third and remaining term is taken as the difference between the total power input and the other two terms. This is the thermal energy imparted to the pool by anodic surface heating. In equation form,[11]

$$P_{\text{arc}} = I_b V_b - (dm/dt)h_{\text{sup}} - (1 - C_b)I_b V_e \qquad [1]$$

where, P_{arc} is the arc thermal power, I_b is the buss-bar current, V_b is the buss-bar voltage, dm/dt is the melt rate, h_{sup} is the enthalpy to superheat temperature, C_b is the fraction of bus-bar current entering the pool surface ($I_{\text{pool}}/I_{\text{b}}$, or, the current efficiency), and V_e is the average anodic surface voltage drop ($V_e \cong 1/2\ V_b$). The distribution of the arc current and the thermal energy on the pool top are each represented by separate Gaussian distributions, which are specified by entering a characteristic "radius"' into the model-parameter table. The arc characteristics and side and bottom thermal and electrical profiles used in the macromodel were chosen based on measured values, followed by a calibration procedure to fit the predicted melt-pool depth and the extent of the mushy zone (characterized by the secondary dendrite arm spacing) to experimental observations.

The thermal predictions from the macromodel were then fed into the CA mesomodel as a postprocessing operation. In the mesomodel, grain nucleation is modeled using a stochastic nucleation model. Once nucleated, grains grow according to the KGT model.[31] Crystallographic anisotropy of grains is considered *via* a decentered square-growth algorithm adapted from the original concepts of Gandin and Rappaz.[32] The thermophysical data used in the mesomodel, including nucleation and growth parameters, were derived from prior studies.[10]

The entire morphology of the grain structure predicted by the VAR multiscale model, including crystallographic orientation, was transferred to the homogenization model, as described subsequently.

C. *Homogenization Heat Treatment*

A quantitative simulation of normal grain growth during this heat-treatment operation was performed using a CA model.[14] The CA model is based on a discrete solution on a mesoscopic scale of the classical Turnbull rate equation for grain-boundary motion. In equation form,[14]

$$v = m_0\gamma_0\kappa \sin(\theta)[1 - \ln(\sin(\theta))]\exp\left(-\frac{Q_\alpha}{RT}\right) \qquad [2]$$

where m_0 is the pre-exponential factor of the boundary mobility, γ_0 is the maximum grain-boundary energy seen at the maximum grain-boundary misorientation of θ (*e.g.*, $\pi/2$), κ is the grain-boundary curvature, Q_a is the activation energy for grain-boundary motion, R is the universal gas constant, and T is the temperature in Kelvin. The CA rules were used to determine the state of each cell based on the local driving force. As can be seen from Eq. [2], the effects of both the boundary curvature and the grain misorientation were incorporated. The driving force was used to determine the direction of the movement of each boundary cell, forming the basis of a continuous variable-cell transition rule.

The homogenization model allows the effects of various stages of the heat treatment (*e.g.*, temperature, ramp rate, and hold time) on grain growth to be simulated, reducing the need for extensive experimental test matrices. Through these simulations, the homogenization process can be further optimized to engineer grain structures appropriate for the subsequent forming processes. The grain-size information for the homogenized ingot was transferred as an initial condition for the cogging model, as described subsequently.

D. *Cogging*

Development of models capable of predicting microstructural changes during the cogging process guides the optimization of both the resultant mechanical properties in the final disc component and quality-control procedures, such as ultrasonic inspectability. A robust, experimentally validated, constitutive model describing the flow stress of alloy 718 under a range of conditions representative of industrial cogging processes[15] was developed and integrated into the DEFORM3D (Scientific Forming Technologies Corporation) finite-element package as a user subroutine. The constitutive model identifies the critical microstructural transitions and corresponding changes in flow stress during hot working following the relationships developed by Evans[15] and Sellars–Tegart.[33]

$$\sigma = \frac{1}{\alpha}\sinh^{-1}\left\{\left[\frac{\dot{\varepsilon}}{A}\exp\left(\frac{Q_{\text{DEF}}}{RT}\right)\right]^{1/n'}\right\} \qquad [3]$$

where σ is the flow stress and $\dot{\varepsilon}$ is the strain rate. The parameters α, A, n', and Q_{DEF} are experimentally determined material constants which can be used to relate changes in flow stress to the strain rate and deformation temperature. Characteristic decreases in the flow stress or softening due to dynamic recrystallization/adiabatic heating were restricted to deformation occurring above both a critical strain ($\varepsilon_{\text{CRIT}}$) and strain rate ($\dot{\varepsilon}_{\text{CRIT}}$). Following a critical strain, the rate of dynamic recrystallization ($\dot{r}$) and the volume fraction of recrystallized alloy (V_{DRX}) for each specified time increment (Δt) can be expressed as:

$$\dot{r} = \frac{dV}{d\varepsilon} = D\dot{\varepsilon}^q \exp\left(\frac{Q_{\text{DRX}}}{RT}\right) \qquad [4]$$

$$V_{f(\text{DRX})} = 1 - (1 - V_{i(\text{DRX})})\exp(-\dot{r}\dot{\varepsilon}\Delta t) \qquad [5]$$

The parameters D and q are material constants, while Q_{DRX} is the activation energy associated with dynamic recrystallization. The terms $V_{f(\text{DRX})}$ and $V_{i(\text{DRX})}$ correspond to the final and initial fractions of the microstructure, respectively, that have dynamically recrystallized during the time increment.

Under processing conditions where dynamic recrystallization does not occur, strain is accumulated until a critical level is obtained to initiate static recrystallization. The extent of grain growth is governed by the thermal history, and the Avrami relationship describes the recrystallized volume fraction (V_{SRX}).

$$V_{\text{SRX}} = 1 - \exp(-kt^n) \qquad [6]$$

Here, k and n are material constants associated with the recrystallization kinetics of alloy 718. Experimentally validated

relationships for predicting the size of the recrystallized grains and the kinetics of grain growth for alloy 718[34,35,36] were coupled to the numerical cogging model.

E. *Forging*

Mechanisms governing the complex mechanical, microstructural, and thermal evolution of the metal during forging are essentially identical to those in cogging. Despite the similarities, a slightly different approach was taken to model the microstructural changes occurring during forging. The radial symmetry of the disc geometry reduced the computational complexity to a two-dimensional axisymmetric finite-element simulation. Dedicated user subroutines were implemented into DEFORM2D (Scientific Forming Technologies Corporation) to accurately predict the high-temperature, rate-dependent deformation characteristics and associated changes in microstructure due to recrystallization and grain growth. In this case, a state variable model incorporating microstructural parameters was utilized to accurately predict the mechanical flow behavior of the metal during forging.[37] Model equations were formulated in terms of the evolution of an internal back stress (σ_b), which is related to the hardening and recovery associated with the formation of dislocation networks, and to the kinetics of dynamic recrystallization. With the dominant deformation mechanisms that are operative during conventional forging operations of Ni-based superalloys being identical to those corresponding to high-temperature creep, this behavior can be described using a modified power-law creep equation.

$$\dot{\varepsilon} = B(\sigma - \sigma_b)^m \exp\left(\frac{-Q_{\text{FORGE}}}{\text{R}T}\right) \quad [7]$$

The constant (B), stress exponent (m), and activation energy (Q_{FORGE}) are material parameters unique to alloy 718. Carefully controlled isothermal compression-test data were used to calculate a global set of parameters valid for the present analyses.

$$\sigma_b = \sigma_\rho + \sigma_g \quad [8]$$

The back stress (σ_b) consists of two terms: one controlled by the dislocation density (σ_ρ) and the other by the grain size (σ_g). Since dynamic recrystallization occurs during deformation, the backstress is a weighted fraction of σ_ρ and σ_g accounting for both the recrystallized and deformed regions of the microstructure.

$$\sigma_\rho = \mu \mathbf{b} \sqrt{\rho}\,(1 - V_{\text{DRX}}) + \mu \mathbf{b} \sqrt{\rho_o} V_{\text{DRX}} \quad [9]$$

$$\sigma_g = 0.1 d_o^{-1/2}(1 - V_{\text{DRX}}) + 0.1 d_{\text{DRX}}^{-1/2} V_{\text{DRX}} \quad [10]$$

where μ is the shear modulus, $\mathbf{b}$ is the Burgers vector, d_o is the initial grain size, d_{DRX} is the dynamically recrystallized grain size, and ρ and ρ_o are the dislocation densities corresponding to the deformed and recrystallized regions, respectively. These relationships allow prediction of the microstructure based on the characteristic changes in flow stresses as a function of temperature and strain rate. The state variable model also enables quantification of the mechanisms resulting in dynamic and metadynamic recrystallization. Compared to the phenomenological relationships used to model the microstructural changes during cogging, the state variable model used in the forging analysis possesses significantly better predictive capability. However, due to the severe computational requirements associated with the three-dimensional cogging simulations and the incremental nature of the hot-deformation process, the state variable model was not applied to simulate the cogging process.

The model equations and finite-element subroutines were validated using a number of small-scale and industrial forging trials. To retain microstructural information generated from the previous processing stages, predicted grain sizes from the cogging simulations were extracted from the three-dimensional mesh of the billet on an element-by-element basis and reformulated as a simple function of billet radius. This was then used to set up the initial grain-size distribution in the two-dimensional axisymmetric mesh used in the forging simulation.

F. *Heat Treatment*

The formation and subsequent relaxation of residual stresses associated with the quench from the solution temperature and aging treatment, respectively, was modeled using a thermoelastic-plastic analysis in DEFORM2D. Material properties appropriate to solution heat-treated INCONEL* alloy 718, both previously assessed from the literature and determined experimentally, were established.[38] Due to the sensitivity of the model parameters to microstructural variations, tensile properties of the as-solutioned material used in the industrial-scale validation trials were assessed over a range of temperatures. Pertinent properties, such as the variation in yield stress, were incorporated into the model. Temperature-dependent surface cooling coefficients (h) were obtained by using the measured temperature profile of an immersion-quenched INCONEL alloy 718 rod as a boundary condition in a finite-element model,[38] where the thermal flux (q) is related to the temperature difference between the water and the surface (ΔT) by $q = h\Delta T$.

*INCONEL is a trademark of INCO Alloys International, Huntington, WV.

Quantification of the residual stress field enables optimization of the machining operations to prevent distortion of the disc as highly stressed material is removed. Since these critical structural components are required to adhere to exceedingly fine tolerances, even minor distortions may result in nonconformance. Residual stress states in structural components were also used for assessment of fatigue properties and component-life predictions. Accurate residual-stress predictions allow relaxation of design conservatism, contribute significantly to component life extension, and provide other cost-reduction opportunities. Furthermore, due to the high costs associated with the intermediate processing steps and the inability to recover these costs in nonconforming discs, rejection of components during the final stages of manufacture is extremely undesirable.

III. RESULTS AND DISCUSSION

A. *Grain-Structure Evolution during the Individual Processes*

An industrial-scale VAR trial was instrumented to monitor a number of macroscopic process variables (*e.g.*, current,

voltage, melt rate, wall heat, and current fluxes[11,39]) during the production of a 510-mm-diameter ingot of INCONEL 718. In the simulation, the arc focus was set to 350 and 170 mm for the thermal and electrical fluxes, respectively. The other parameters and thermophysical properties, developed in a previous article,[11] are listed in Table I. The temperature distribution as a function of time generated by the macromodel was passed into a mesoscale CA model to simulate different microstructural features. This CA model tracks the average grain size, distribution, morphology, and texture, indicating, for example, the conditions leading to a transition from columnar to equiaxed grain growth. The predicted grain structure is compared with the experimentally observed structure in Figure 1. The fluid flow in the molten pool and isotherms marking the equilibrium liquidus temperature and undercooled region are shown. The scale and structure of the equiaxed and columnar regions predicted by the mesoscale model qualitatively compares well to those observed experimentally. However, the width of individual columnar grains is overpredicted, because the axisymmetric simulation favors grain overgrowth. The predicted melt-pool shape matches that experimentally measured from tree rings (chains of fine equiaxed grains among a predominantly columnar dendritic structure), shown as a black line in Figure 1(a).[40]

A practical application of such a multiscale VAR model is to explore the influence of modifying the operational process conditions on the predicted grain structure as well as the formation of grain features. These types of sensitivity studies guide cost-effective optimization of the processing parameters. Increasing the melt rate increases the heat input and deepens the molten pool.[11] This decreases the temperature gradient in front of the advancing solid and refines the grain structure. On the other hand, decreasing the melt rate shortens the molten pool and increases the temperature gradient, resulting in a completely columnar structure with only a 25 pct decrease in melt rate. On a microstructural level, good agreement of size, shape, and grain-size distribution was also achieved between the tree rings predicted by the multiscale VAR model with those observed experimentally by the electron backscattered diffraction technique.[10]

Table I. Simulation Parameters Used in the Multiscale VAR Model

Property	Value	Units
Finite-Difference Macromodel		
Ingot radius	0.255	m
Ingot height (to reach steady state)	1.02	m
Electrode radius	0.217	m
Power	144.9	kW
Efficiency of power	45.0	pct
Current	6.3	kA
Volts	23	V
Electrical arc focus	0.17	M
Thermal arc focus	0.35	M
Melt rate	6.47×10^{-2}	kg/s
Casting speed	4.23×10^{-5}	m/s
Turbulence factor	60	pct
Gap formation temperature	1503	K
Temperature of mold wall	400	K
Cell size	8.5×10^{-3}	m

Heat-Transfer Coefficient Estimates at the Ingot/Crucible Interface							
T (K)	500	750	1000	1250	1400	1485	>1570
h_c (W/m^2 K)	20	34	57	107	192	317	70

CA Mesomodel		
Nucleation-curve centroid	18.0	K
Nucleation-curve distribution	1.5	K
Maximum grain density	$2 \times 10^{+9}$	1/m^3
Growth coefficient	1×10^{-7}	m/s/K
Cell size	5.1×10^{-4}	m
Time step	5	s

Grain-structure predictions from the multiscale VAR model were used as the initial state of the heat-treatment model. Simulations of the predicted grain structure before and after a standard heat-treatment operation, consisting of 24 hours at 1160 °C followed by 72 hours at 1200 °C, are compared with the experimental observations in Figure 2. The simulated as-homogenized grain structure (Figure 2(d)) is in good qualitative agreement with the experimental observations (Figure 2(c)). However, the model overpredicts the size of the grains in the outer zone (*e.g.*, 35 *vs* 15 mm). Two possible reasons for this overprediction are (1) the two-dimensional axisymmetric approximation does not account for grains coming in or out of the plane; and (2) the VAR model grid was too coarse to capture the very fine grains in this region.

Microstructural changes during cogging of a 510-mm-diameter ingot of alloy 718 were simulated by transferring the grain-structure information from the homogenization model onto the three-dimensional mesh representing the billet. Model parameters were selected to be representative of industrial cogging processes used at Special Metals–Wiggin (Hereford, United Kingdom). Die velocities were set at 40 mm/min, and the initial working temperature of the billet was 1120 °C. Predictions of the average grain-size distributions after a partial and full reduction in diameter are shown in Figure 3. For the partial reduction, 21 deformation passes with longitudinal rotations of 90 or 45 deg after each pass were simulated to reduce the diameter of the ingot from 510 to 350 mm. As predictions of the average grain size are calculated using the relative volume fraction of fine recrystallized grains with the grain size associated with the corresponding fraction of unrecrystallized matrix, results for the initial stages of cogging are influenced by the initial grain structure of the homogenized ingot (Figure 2). Incomplete recrystallization near the surfaces of the partially cogged billet resulted in slightly larger average grain sizes at those regions (Figure 3). These predicted grain sizes are in close agreement with the experimentally measured values (*e.g.*, 217 *vs* 182 μm in the center). To complete the cogging simulation, the diameter of the partially cogged billet was further reduced to 218 mm *via* a series of 16 deformation passes following a billet reheat at 1040 °C. These additional hot-deformation steps further refine the microstructure to yield a uniform fine-grained microstructure (Figure 4). As the hot-deformation temperatures gradually decrease, precipitation of δ occurs along the boundaries of recrystallized grains and restricts growth.[41] These microstructural transformations are not captured in the existing grain model and tend to result in conservative predictions of grain growth. Despite the complexity of the thermal and deformation boundary conditions, excellent agreement exists

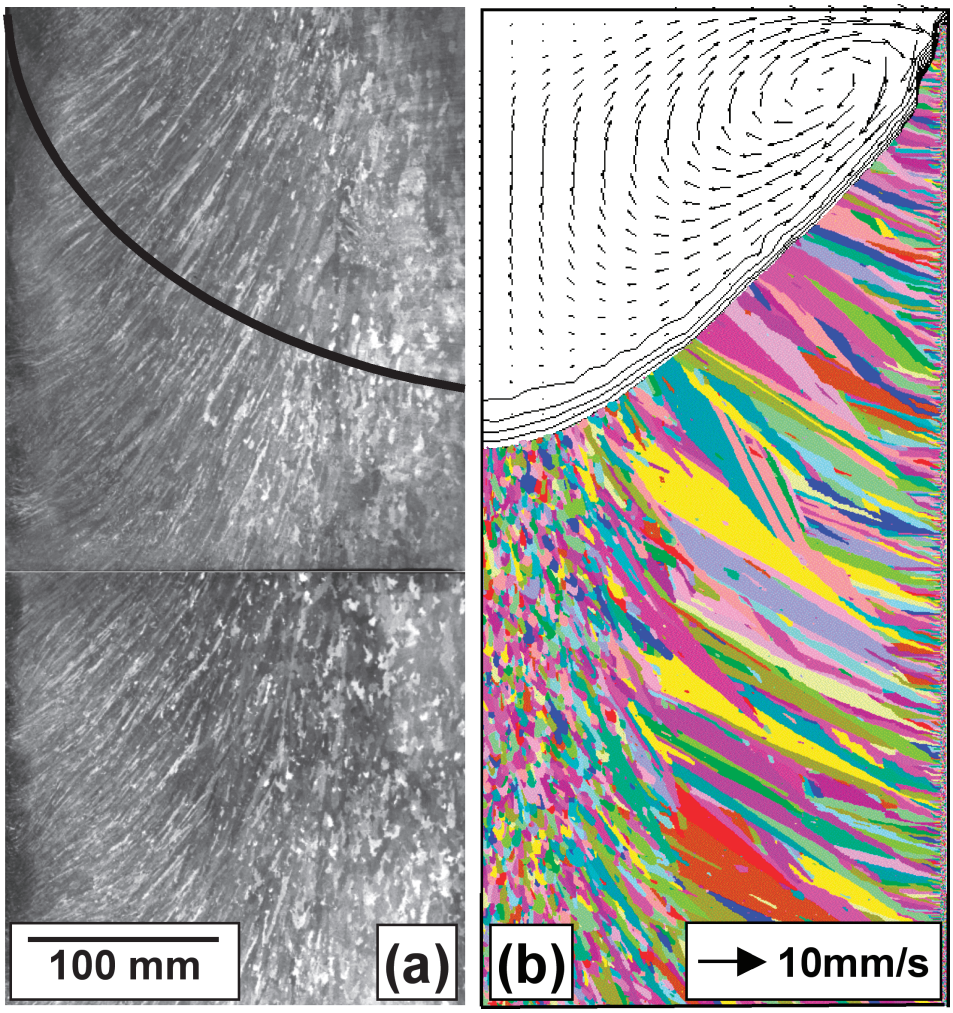

Fig. 1—Comparison of the (*a*) grain structure present in a VAR ingot with the (*b*) grain structure predicted using the multiscale solidification model.

between the grain-size model predictions and experimental measurements in the finished billet (*e.g.*, 87 *vs* 20 μm in the center).

The predicted grain sizes from the cogging simulations were extracted from the three-dimensional mesh of the billet and reformulated as a simple function of billet radius. This was then used to set up the initial grain-size distribution in the two-dimensional axisymmetric mesh used in the forging simulation. The predicted average grain-size distributions after forging with a die speed of 50 mm/s are shown in Figure 5. Complete recrystallization occurs throughout most of the workpiece, and the resulting grain sizes are approximately 10 to 20 μm in diameter (ASTM 8-10). Since much of the forging recrystallizes dynamically or metadynamically, variations in initial billet grain size have little influence on the resulting recrystallized microstructure. Note that *dead* zones, or unrecrystallized regions that retain the original billet grain structure, persist near the center and extremities of the forging and in regions of high die curvature; however, their presence is confined to noncritical locations within the forging.

Building on the results from the forging model, the magnitude and distribution of residual stresses within the forged disc after the solution and aging treatments were predicted.[42] In the model, a disc solutioning temperature of 970 °C was used, and the sink (water) temperature was assumed to be 20 °C. Postquenching, the simulation reveals the presence of residual compressive stresses along the surface of the disc and tensile residual stresses within the interior of the disc. As expected, the magnitudes of the residual stresses predicted at room temperature are similar to the yield stresses measured for the as-solutioned material (Figure 6(a)).

Neutron-diffraction measurements using the ENGIN-X instrument at the ISIS facility in the Rutherford Appleton Laboratories in Oxfordshire, United Kingdom, were performed to validate the residual stress predictions. Measurements of the full-stress tensor[42] were made along the two axial sections through the disc, one near the bore at point AB, and one at the rim at point EF (Figures 6(b) and (c)). Confidence limits for the internal-stress determination that have been calculated from the uncertainty in the lattice parameter were determined using a least-squares peak-fitting package, the General Structure Analysis System. Consistent with the model predictions, the major stresses are the hoop and radial stresses, with the axial stresses being smaller, within the range of 100 MPa tensile to 200 MPa compressive.

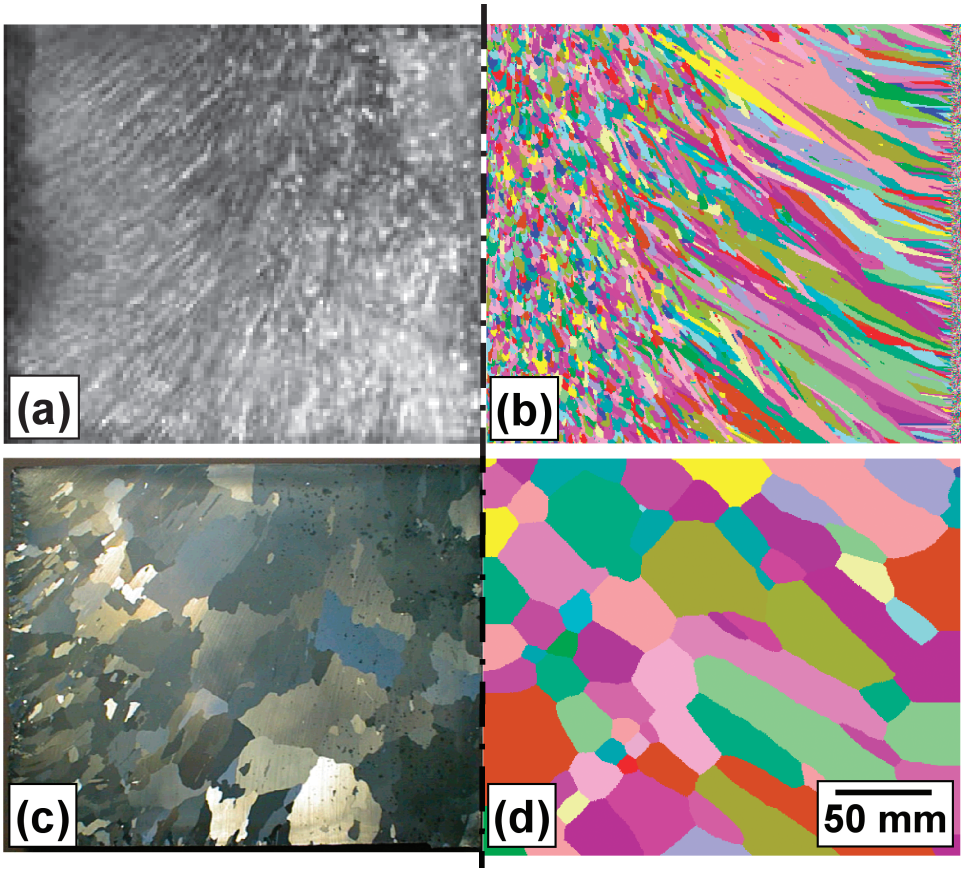

Fig. 2—Comparison of the experimental and simulated grain structure of the ingot, respectively, (*a*) and (*b*) in the as-VAR condition and (*c*) and (*d*) after a homogenization heat treatment.

The hoop and radial stresses are compressive at the surface (up to 600 MPa) and tensile in the core of the disc (up to 400 MPa). The magnitude of the through-thickness stress measurements at the disc rim (point EF) are generally larger than the radial stresses at the disc bore (point AB), as seen in Figures 6(b) and (c).

B. *An Integrated Process Model*

Integration of the various discrete process models enabled the simulation of the entire manufacturing process associated with the production of an INCONEL 718 aeroengine disc. At every opportunity, model predictions were validated against industrial-scale trials by tracking the changes in grain structure from solidification through to final forging. Experimentally measured and predicted radial grain-size distributions at various stages of processing are compared in Figure 7. Extremely good agreement exists at each of the various processing stages. One of the major advantages of the integrated model is the ability to retain and transfer simulation results and data between each link of the through-process simulation. In practice, pertinent materials-processing information is not always retained, as multiple organizations are often enlisted to provide specific processing services. In this particular instance, the industrial-scale VAR melting trials, homogenization, and cogging operations were performed at the Special Metals–Wiggin facility prior to forging, and the heat treatment was performed at the Wyman–Gordon facility. The forging blank was then passed onto Rolls–Royce plc for the final machining operations. The present model consolidates each of these individual activities and enables the impact of each processing operation to be systematically tracked and optimized in an integrated modeling scheme.

The formation and coarsening of the heterogeneous VAR grain structure during solidification and homogenization was accurately simulated in the present model. Critical microstructural parameters, such as solidification textures and local grain-size information were retained and transferred to each of the subsequent stages. Since the homogenization model utilizes existing grain-structure textures developed during solidification to model the degree of grain growth at elevated temperatures, data transfer between the processing stages is required for accurate predictions. Following homogenization, microstructural information was also transferred into the thermomechanical processing models. Although both flow properties and recrystallization mechanisms are sensitive to the grain size, sufficiently high levels of deformation were utilized during cogging to produce a uniform and fine-grained microstructure (Figure 4). Finally, the grain structure was further refined in the forging process to yield an average grain size between 10 and 30 μm, although there are isolated dead zones that contain grains as large as 100 to 120 μm. Despite being highly undesirable, the characteristic locations of these dead zones within the forging enable them to be effectively removed from the finished component during the machining stage.

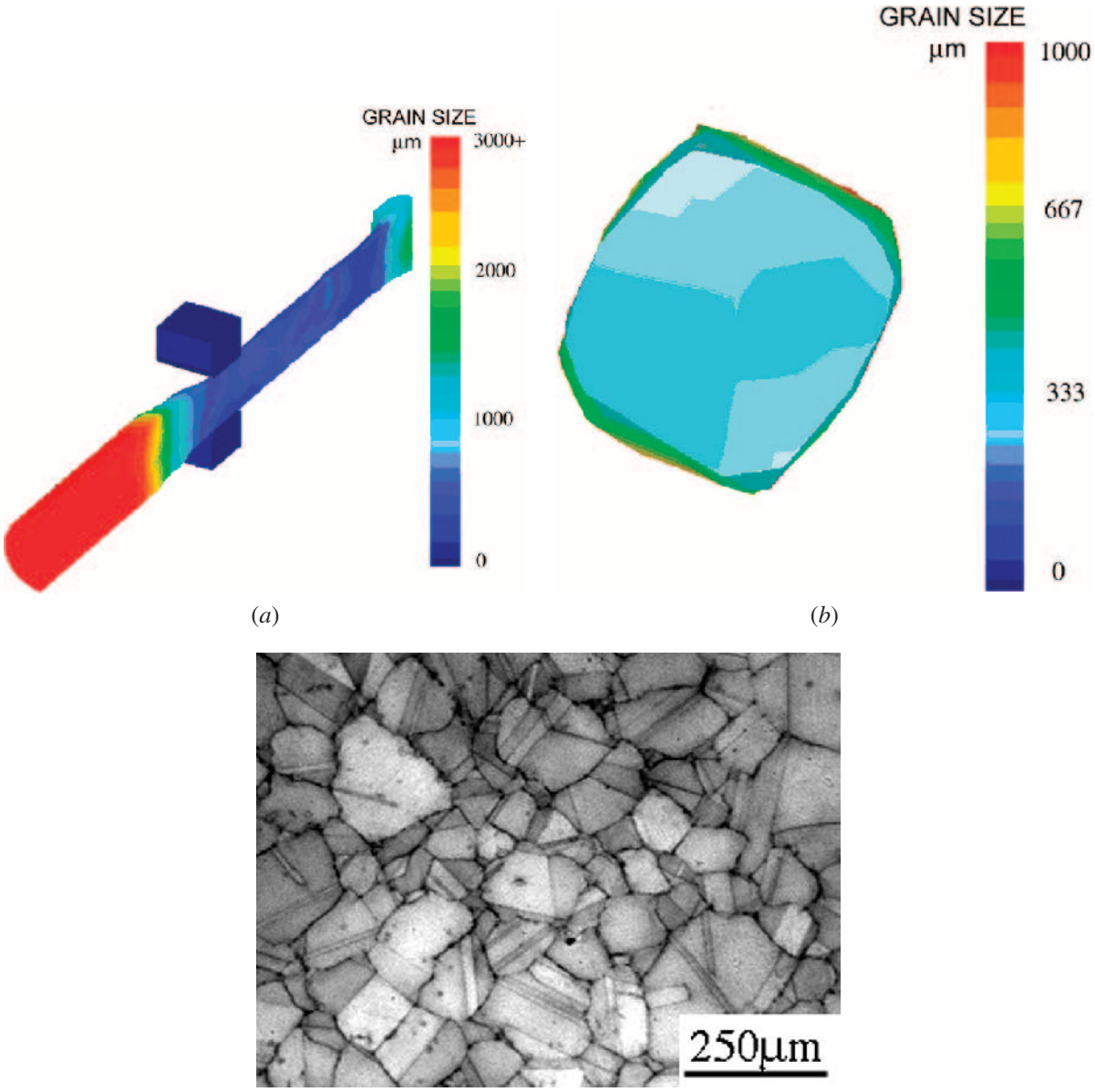

(*a*) (*b*)

(*c*)

Fig. 3—Predicted grain-size distributions along the (*a*) longitudinal and (*b*) transverse sections of the ingot after a partial reduction in diameter. Substantial grain refinement occurs during hot working as the diameter of the ingot is gradually reduced from 508 to ~350 mm. (*c*) Actual grain structure of the partially reduced ingot.

In addition to grain-structure information, the integrated process model also allows other aspects of the component structure to be tracked during manufacture. Since the model provides a comprehensive thermomechanical deformation history of the finished component, retained strains in complex structural forgings can also be predicted. With these residual strains often leading to microstructural irregularities due to abnormal grain growth during the solutioning heat treatment, monitoring and developing processes capable of minimizing these effects becomes possible through the use of the integrated model. Moreover, tracking the locations of macroscopic inclusions and other deleterious defects introduced at various stages of manufacturing also becomes viable with the model. As detailed in the following section, data transfer between the various models enables the design of robust and cost-effective manufacturing processes for the production of aeroengine turbine discs.

C. *Defect Tracking during Manufacture*

The structural properties of aeroengine discs are highly sensitive to the presence of localized compositional or microstructural heterogeneities. Common solidification defects present in VAR ingots (Figure 8) may include crown fall-in, freckles, white spots, splash, and steel shot.[9] Since the presence of any of these defects within the final disc can potentially lead to premature and catastrophic failure of the component, preventing the occurrence of these defects in the final component is of vital importance. For certain aerospace discs, the formation of these processing defects can

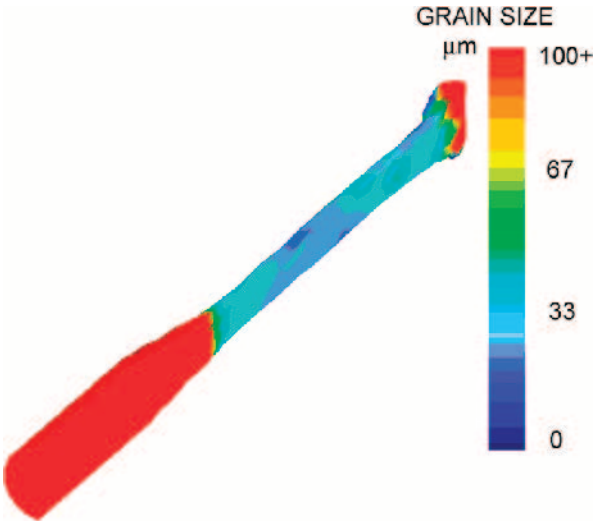

(*a*)

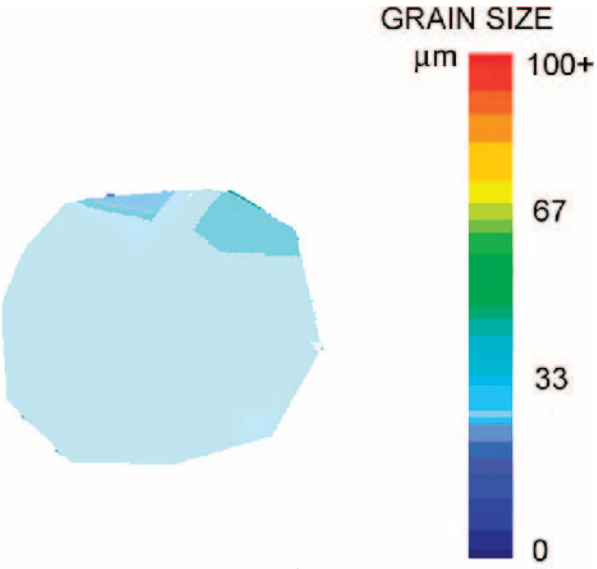

(*b*)

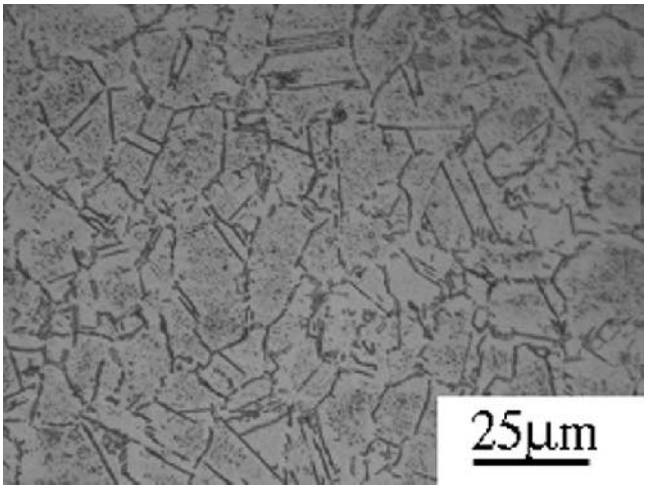

(*c*)

Fig. 4—Predicted grain-size distributions along the (*a*) longitudinal and (*b*) transverse sections of the ingot after a full reduction in diameter. Average grain sizes are further refined during hot working as the diameter of the ingot is reduced to a final diameter of 225 mm. (*c*) Microstructure of the fully cogged ingot, revealing the presence of grain boundary δ and intragranular γ''.

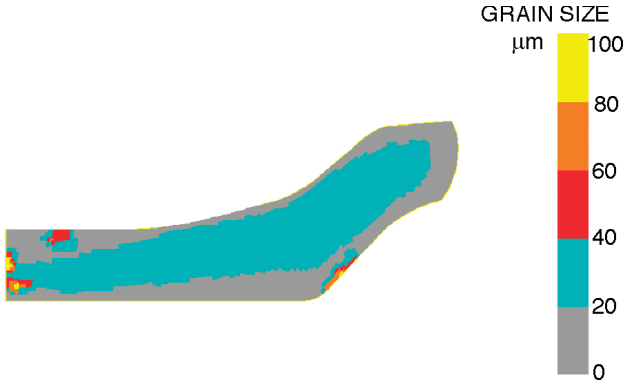

(*a*)

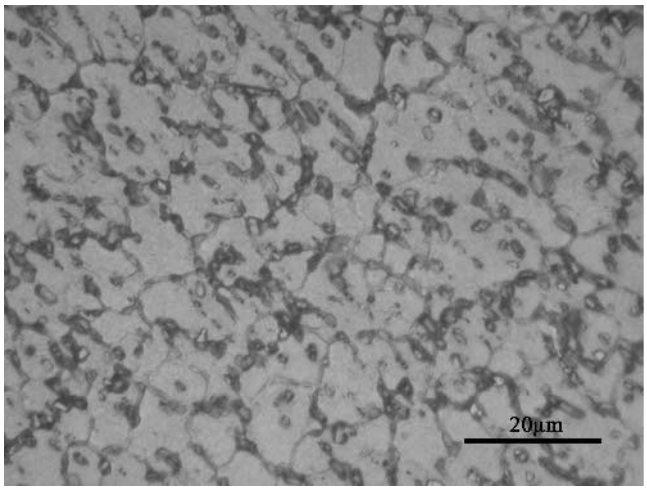

(*b*)

Fig. 5—The average (*a*) predicted grain-size distribution in the disc after forging and (*b*) micrograph revealing the actual grain structure of the forging.

be suppressed through careful control of the VAR process. Since the susceptibility to the formation of these defects increases with VAR ingot size, the production of defect-free ingots for large industrial gas turbines for power-generation applications becomes extremely challenging. In these instances, tracking the location of potential defects during processing enables the development of cost-effective and intelligent forging and machining operations that are able to minimize the occurrence of defects within the finished component and, consequently, relax the safety factors in design.

Defect positions corresponding to all stages of the manufacturing process were monitored through the process simulation. The displacements of potential defects introduced during solidification were systematically tracked during subsequent thermomechanical processing using the integrated modeling scheme. The initial locations of the potential defects in the VAR ingot were represented using four strategically placed points (Figure 9). Point 1 lies near the edge, point 2 in the center, and points 3 and 4 in the midradius. These points correspond closely to the characteristic locations where freckles and white spots are commonly observed in VAR ingots. The movement of these points was tracked through the entire manufacturing route of the disc.

After cogging, it can be seen that points 1 and 2 remain within the same plane, while points 3 and 4 are largely dis-

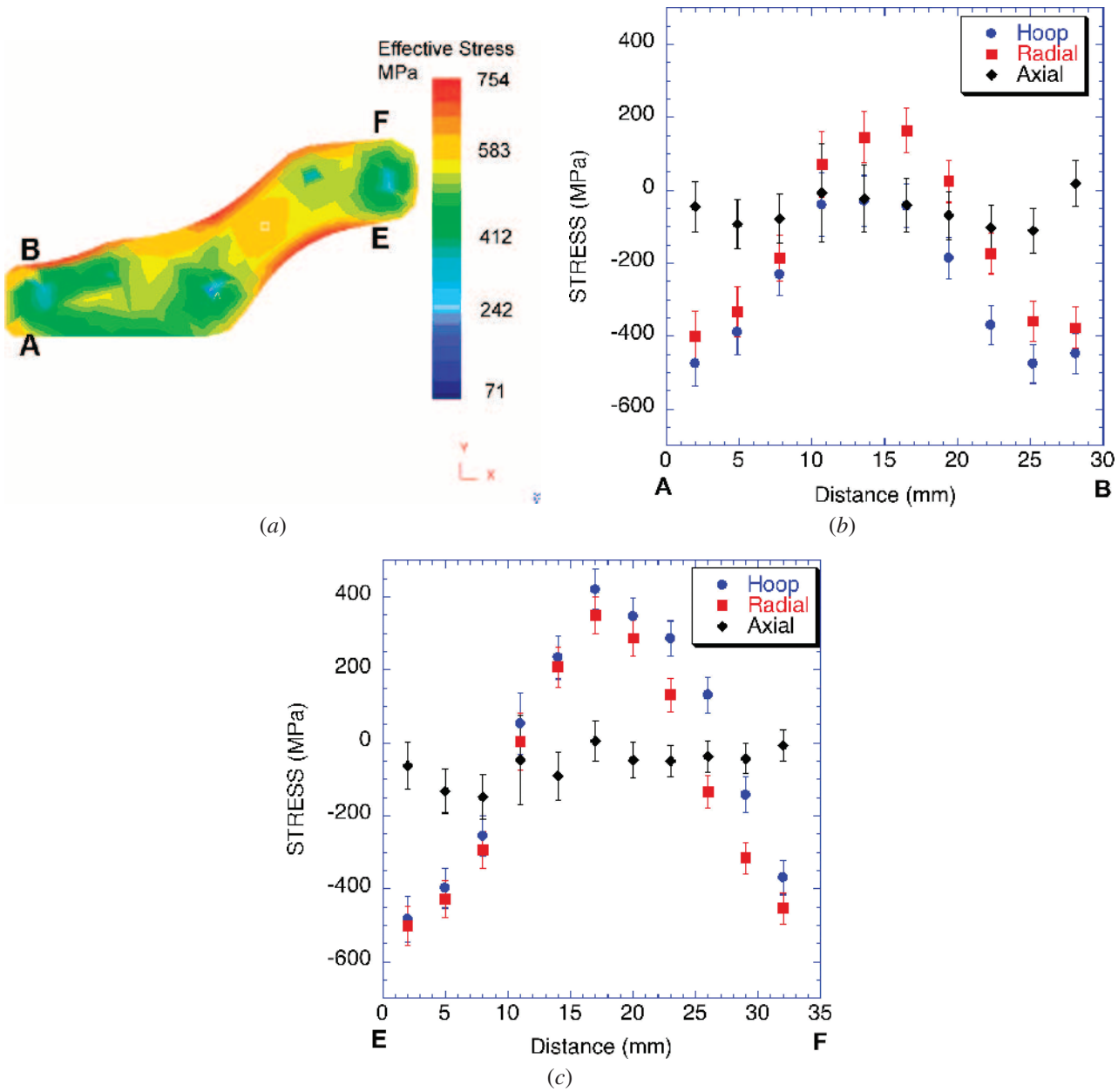

Fig. 6—(*a*) Predicted distribution of residual stresses within the disc forging after water quenching from the solutioning temperature. Through-thickness residual stresses measured at (*b*) the bore (point AB) and (*c*) the rim (point EF) of the disc forging using neutron-diffraction techniques.

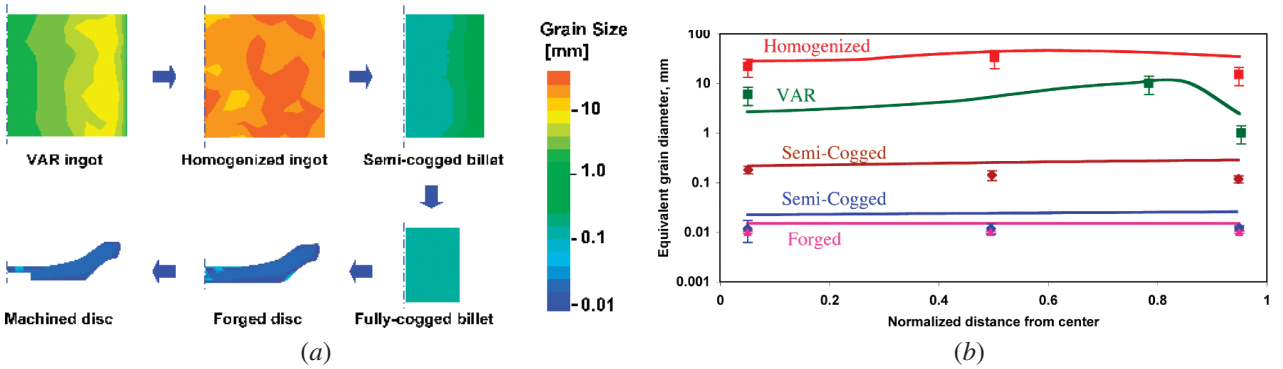

Fig. 7—(*a*) Schematic showing the predicted grain sizes after each processing stage and (*b*) comparison of the experimentally measured grain sizes to the model predictions. Good agreement exists at all stages of the integrated model.

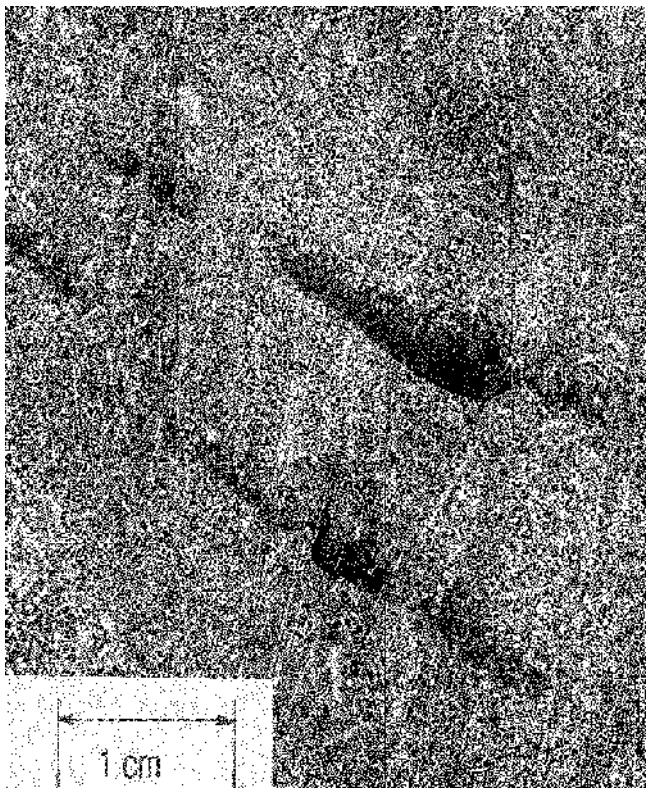

(*a*)

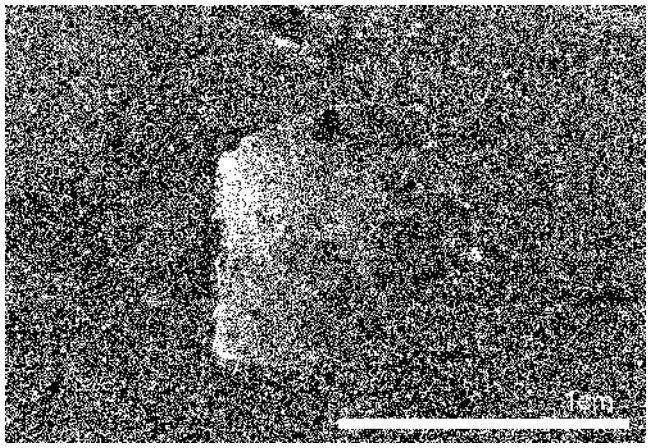

(*b*)

Fig. 8—Micrographs of common (*a*) freckle and (*b*) white-spot defects observed in vacuum-arc remelted ingots of INCONEL alloy 718.

placed from each other in the elongated billet. The relative radial locations of all these points remained the same as in the original ingot. A cylindrical section of the cogged billet containing all of these points was then subjected to the forging simulation.

Following forging, point 1 is displaced very close to the disc surface, while point 2 remains at its original location in the center. Point 3 is displaced toward the top surface and could result in a subsurface defect. Point 4 remains inside the disc. After the final machining, points 1 and 2 are completely removed from the disc, while points 3 and 4 still

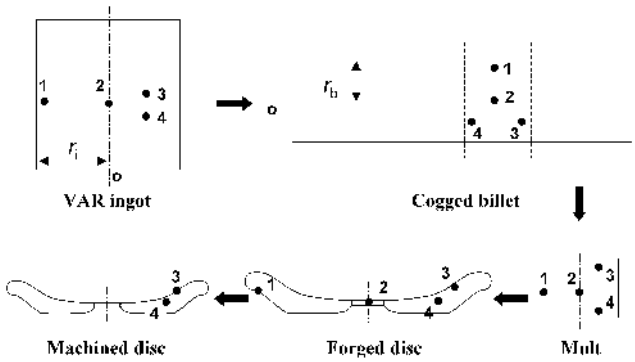

Fig. 9—Schematic illustrating the defect-point tracking capability of the integrated model. Points representing defects in the vacuum-arc remelted ingot can be effectively tracked through the entire manufacturing route.

remain within the disc and represent typical subsurface and embedded defects in the disc, respectively.

The simulated defects may greatly influence the structural integrity of the disc. Defects located near the surface (*e.g.*, point 3) are likely to serve as crack-initiation sites and lower the fatigue resistance. The presence of internal inclusions, such as point 4, may potentially serve as stress concentrators and enhance crack-propagation rates. For this particular disc geometry, the existence of midradius defects such as freckles and discrete white spots in the VAR ingot is clearly undesirable, as they are likely to remain in the disc. Inclusions and defects located near the center or edge of the VAR ingot have a much higher probability of being removed during final machining. The integrated model can also be used with coordinate-specific information regarding the approximate location of the defects within the billet. This enables billets containing strategically located defects to be forged in a way that the resulting deformation will displace the defects into noncritical regions of the forging that will be subsequently machined away. Hence, cost-effective processes can be developed to minimize the occurrence of defects in the finished component.

Using the integrated process model, it is also possible to perform inverse defect tracking, *i.e.*, tracking defects found in the machined disc back to their original positions in the VAR ingot. The characteristic tendencies for the various defects to reside along certain regions of the VAR ingot enable the model to predict the probable locations of different defects within the finished forging. For example, if ultrasonic testing of the machined disc reveals a subsurface defect at the disc rim, the model could be applied to identify the defect as being either a freckle, discrete white spot, or an extrinsic inclusion, whereas the fully embedded defect at the same radial distance would probably be an extrinsic inclusion. In this manner, the model can be used to improve the quality of the final product by tracking the source of any observed defects and minimizing their occurrence, for example, through improved process control.

IV. CONCLUSIONS

An integrated process model has been developed to track grain structure/defects as they evolve and move position during the complex manufacturing chain for gas-turbine discs of INCONEL alloy 718. The model encompasses all of the

process stages from ingot production by VAR through the intermediate manufacturing stages of homogenization, cogging, forging, and heat treatment. The model shows that although the grain structure of the alloy changes significantly throughout different stages of the process, the final grain structure at each stage is related to that formed in the previous stages. The ability of the model to accurately predict the occurrence and locations of defects (*e.g.*, inclusions, freckles, and white spots) greatly enhances the tracking capabilities through the production chain. This integrated model permits sensitivity studies to be performed to predict the robustness of processing parameters, to ensure that defects cannot arise even in the presence of quantified process variability. The model also provides guidance on the most important areas to target through process control, both to prevent defect formation and to achieve a desired final grain structure.

The modeling methodology used in constructing the model is currently being adapted to simulate complex manufacturing processes using other alloy systems.

ACKNOWLEDGMENTS

The authors thank their colleagues at Birmingham University (Birmingham, United Kingdom), Special Metals Corporation, Special Metals–Wiggin Ltd., Wyman–Gordon Ltd., Rolls–Royce plc, and QinetiQ. This research was funded in part by the EPSRC (Grant No. GR/N14132 and GR/N14101).

REFERENCES

1. Rolls-Royce plc, Derby, 1986.
2. M. McLean: *Directionally Solidified Materials for High Temperature Service*, The Metals Society, London, 1983, pp. 5-9.
3. A. Kermanpur, S. Tin, P.D. Lee, and M. McLean: *J. Miner. Met. Mater. Soc*., 2004, vol. 56 (3), pp. 72-78.
4. R.M. Forbes Jones and L.A. Jackman: *J. Met*., 1999, vol. 51 (1), pp. 27-31.
5. A.S. Ballantyne and A. Mitchell: *Ironmaking and Steelmaking*, 1977, vol. 4 (4), pp. 222-39.
6. F.J. Zanner, R.L. Williamson, R.P. Harrison, H.D. Flanders, R.D. Thompson, and W.C. Szeto: in *Superalloy 718—Metallurgy and Applications*, TMS, Warrendale, PA, 1989, pp. 17-32.
7. P.D. Lee, R.M. Lothian, L.J. Hobbs, and M. McLean: in *Superalloys 1996*, TMS, Warrendale, PA, 1996, pp. 435-42.
8. P.D. Lee, P.N. Quested, and M. McLean: *Phil. Trans. A*, 1998. vol. 356, pp. 1027-43.
9. W. Zhang, P.D. Lee, and M. McLean: *Metall. Mater. Trans. A*, 2002, vol. 33A, pp. 443-54.
10. X. Xu, W. Zhang, and P.D. Lee: *Metall. Mater. Trans. A*, 2002, vol. 33A, pp. 1805-15.
11. A. Kermanpur, D.G. Evans, R.J. Siddall, P.D. Lee, and M. McLean: *Int. Symp. on Liquid Metal Processing and Casting*, Nancy, France, SFZM, Paris, 2003, pp. 39-47.
12. D. Raabe: *Acta Mater*., 2000, vol. 48, pp. 1617-28.
13. C. Maurice: *Recrystallization and Grain Growth*, Springer-Verlag, Berlin, Germany, 2001, pp. 123-34.
14. A. Kermanpur, W. Wang, P.D. Lee, and M. McLean: *Mater. Sci. Technol*., 2003, vol. 19 (7), pp. 859-65.
15. C.A Dandre, S.M. Roberts, R.W. Evans, and R.C. Reed: *Mater. Sci. Technol*., 2000, vol. 16 (1), pp. 14-25.
16. G.S. Shen, S.L. Semiatin, and R. Shivpuri: *Metall. Mater. Trans. A*, 1995, vol. 26A, pp. 1795-1803.
17. A.J. Brand, S. Kalz, and R. Kopp: *Comput. Mater. Sci*., 1996, vol. 7 (1–2), pp. 242-46.
18. *Controlled Thermo-Mechanical Processing of Tubes and Pipes for Enhanced Manufacturing and Performance*, 1999, www.oit.doe.gov/steel/factsheets/ctmp.pdf.
19. European FP5 Programs G5RD-CT-2000-00153, -1999-00132, and -1999-00155.1999, http://www.eaa.net/downloads/virprojects.pdf.
20. D.M. Maijer, Y.X. Gao, P.D. Lee, T.C. Lindley, and T. Fukui: *Metall. Mater. Trans. A*, 2004, vol. 35A, pp. 3275-88.
21. E. Samuelsson, J.A. Domingue, and G.E. Maurer: *J. Miner. Met. Mater. Soc*., 1990, vol. 42 (8), pp. 27-30.
22. L.A. Jackman, G.E. Maurer, and S. Widge: *Adv. Mater. Processes*, 1993, vol. 143 (5), pp. 18-25.
23. B.K. Damkroger, J.B. Kelley, M.E. Schlienger, J. Van Den Avyle, R.L. Williamson, and F.J. Zanner: *Superalloys 718, 625 and Various Derivatives*, TMS, Warrendale, PA, 1994, pp. 125-35.
24. W. Zhang, P.D. Lee, M. McLean, and R.J. Siddall: *9th Int. Symp. on Superalloys*, TMS, Warrendale, PA, 2000, pp. 29-37.
25. L.A. Bertram, J.A. Brooks, D.G. Evans, A.D. Patel, J.A. Van Den Avyle, and D.D. Wegman: *Int. Symp. on Liquid Metal Processing and Casting*, AVS, Santa Fe, NM, 1999, pp. 156-67.
26. L.A. Bertram, C.B. Adasczik, D.G. Evans, R.S. Minisandram, P.A. Sackinger, D.D. Wegman, and R.L. Williamson: *Int. Symp. on Liquid Metal Processing and Casting*, AVS, Santa Fe, NM, 1997, pp. 110-32.
27. W. Wang, P.D. Lee, and M. McLean: *Acta Mater*., 2003, vol. 51 (10), pp. 2971-87.
28. P.D. Lee, A. Chirazi, R.C. Atwood, and W. Wang: *Mater. Sci. Eng. A–Structural Materials Properties Microstructure and Processing*, 2004, vol. 365 (1–2), pp. 57-65.
29. P.D. Lee, D. See, and R.C. Atwood: *Cutting Edge of Computer Simulation of Solidification and Casting*, ISIJ, Osaka, Japan, 1999, pp. 97-111.
30. R.C. Atwood and P.D. Lee: *Metall. Mater. Trans. B*, 2002, vol. 33, pp. 209-21.
31. W. Kurz, B. Giovanola, and R. Trivedi: *Acta Metall*., 1986, vol. 34 (5), pp. 823-30.
32. C.A. Gandin and M. Rappaz: *Acta Mater*., 1997, vol. 45 (5), pp. 2187-95.
33. C.M. Sellars and W.J.M. Tegart: *Int. Metall. Rev*., 1972, vol. 17 (1), pp. 1-24.
34. L.X. Zhou and T.N. Baker: *Mater. Sci. Eng*., 1994, vol. A177, pp. 1-9.
35. L.X. Zhou and T.N. Baker: *Mater. Sci. Eng*., 1995. vol. A196, pp. 89-95.
36. S.C. Medeiros, Y.V.R.K Prasad, W.G. Frazier, and R. Srinivasan: *Mater. Sci. Eng*., 2000, vol. A293, pp. 198-207.
37. X. Zhao, R.P. Guest, S. Tin, J.W. Brooks, and M. Peers: *Mater. Sci. Technol*., 2004. vol. 20 (11), pp. 1357-66.
38. D. Dye, K.T. Conlon, and R.C. Reed: *Metall. Mater. Trans. A*, 2004, vol. 35A, pp. 1703-13.
39. R.M. Ward and M.H. Jacobs: *Int. Symp. on Liquid Metal Processing and Casting*, Nancy, France, SF2M, Paris, 2003, pp. 49-58.
40. R.M. Ward, T.P. Johnson, and M.H. Jacobs: *Int. Symp. on Liquid Metal Processing and Casting*, AVS, Santa Fe, NM, 1997, pp. 97-109.
41. R.P. Guest and S. Tin: *Parsons 2003 Engineering Issues in Turbine Machinery, Power Plant and Renewables*, Institute of Materials, Minerals and Mining, Dublin, 2003, pp. 703-19.
42. D. Dye, B.A. Roder, S. Tin, M.A. Rist, J.A. James, and M.R. Daymond: *Superalloys 2004*, TMS, Warrendale, PA, 2004, pp. 315-22.